Electronic Supplementary Material (ESI) for CrystEngComm.

Four POM-based complexes modified by multi-nuclear clusters: structures, photocatalytic, supercapacitor and chromogenic properties

Shufang Ma, Jun Ying,* Yanping Zhang, Aixiang Tian*

Table S1. Selected bond distances (Å) and angles (°) for complexes **1**–**4**.

Complex **1**

Cu(1)-N(5)	2.157(2)	Cu(2)-N(4)	1.993(2)
Cu(1)-N(1)	1.961(2)	Cu(2)-N(2)^{2}	2.026(2)
Cu(1)-O(14)	1.9342(18)	Cu(1)-O(11)	2.052(2)
O(14)-Cu(1)-O(14)^{2}	82.53(8)	O(14)-Cu(1)-O(11)	99.21(8)
O(14)-Cu(1)-N(5)	85.86(8)	O(14)-Cu(1)-N(1)	167.77(9)
O(11)-Cu(1)-N(5)	91.52(9)	N(1)-Cu(1)-O(11)	89.41(9)
N(1)-Cu(1)-N(5)	102.68(9)	O(14)-Cu(2)-Cl(1)	170.68(6)
O(14)-Cu(2)-N(4)	89.84(9)	N(4)-Cu(2)-Cl(1)	95.04(7)
N(4)-Cu(2)-N(2)^{2}	150.73(10)	N(2)^{2}-Cu(2)-Cl(1)	93.49(7)

Symmetry codes for **1**: ^{1}1-X, -Y, 1-Z; ^{2}-X, 1-Y, 1-Z

Complex **2**

Cu(1)-O(1W)	1.971(9)	Cu(1)-N(1)	1.997(10)
Cu(1)-O(3W)	1.978(14)	Cu(1)-N(5)	1.949(11)
Cu(1)-O(2W)	2.332(13)	N(5)-Cu(1)-N(1)	166.8(5)
N(5)-Cu(1)-O(1W)	90.5(5)	O(1W)-Cu(1)-N(1)	94.5(5)
N(5)-Cu(1)-O(2W)	100.1(5)	O(3W)-Cu(1)-N(1)	83.6(5)

Complex **3**

Cu(1)-N(5)	2.027(6)	Cu(2)-N(6)	1.984(6)
Cu(1)-N(3)	2.052(7)	Cu(2)-N(6)^{1}	1.984(6)
Cu(1)-N(9)	1.960(8)	Cu(2)-N(4)1	1.975(6)
N(5)-Cu(1)-Cl(1)	86.2(2)	N(6)^{1}-Cu(2)-N(6)	180.0(3)

N(5)-Cu(1)-N(3)	90.8(3)	N(4)-Cu(2)-N(6)^{1}	90.5(3)
N(3)-Cu(1)-Cl(1)	174.4(2)	N(4)-Cu(2)-N(6)^{1}	89.5(3)
N(9)-Cu(1)-Cl(1)	88.7(3)	N(4)^{1}-Cu(2)-N(6)	90.5(3)
N(9)-Cu(1)-N(5)	174.6(3)	N(4)-Cu(2)-N(6)	89.5(3)
N(9)-Cu(1)-N(3)	94.5(3)	N(4)-Cu(2)-N(4)^{1}	180.00(3)

Symmetry codes for **3**: ^{1}1-X, 1-Y, 1-Z

Complex **4**

Co(1)-N(9)	2.078(5)	Co(1)-N(1)	2.076(5)
Co(1)-N(6)	2.142(5)	Co(1)-O(22)	2.125(4)
Co(1)-N(9)	2.078(5)	Co(1)- O(21)^{3}	2.038(5)
Co(2)-N(2)^{4}	2.166(5)	Co(2)-N(2)	2.166(5)
Co(2)-N(10)	2.125(5)	Co(2)-N(5)	2.172(5)
N(9)-Co(1)-O(22)	175.98(19)	N(9)-Co(1)-N(6)	87.7(2)
N(1)-Co(1)-N(9)	95.2(2)	N(1)-Co(1)-N(6)	90.4(2)
N(2)-Co(2)-N(5)	88.9(2)	N(2)-Co(2)-N(5)^{4}	91.1(2)
N(10)-Co(2)-N(2)^{4}	88.5(2)	N(10)-Co(2)-N(5)	86.7(2)

Symmetry codes for **4**: ^{1}2-X, 1-Y, 2-Z; ^{2}1-X, -Y, 1-Z; ^{3}1-X, 1-Y, 1-Z; ^{4}-X, 1-Y, 1-Z

Ligand syntheses

Synthesis of Tpm: Formaldehyde hydrazide (6 g) was dissolved in 200 ml methanol, triethyl orthoformate (33 ml) was added and refluxed at 75 ^{o}C for 2 hours. Then N-(3-aminopropyl)-morpholine (7.3 ml) was added and refluxed for 4 hours.

Synthesis of Cmt: Triazole (1.4 g) was dissolved in 35 ml ethanol, and 0.47 g of Na wire was added. When the sodium wire was completely dissolved, 2 ml of chloromethylcyclopropane was added. The solution was stirred well, and refluxed for three days at 78 ^{o}C.

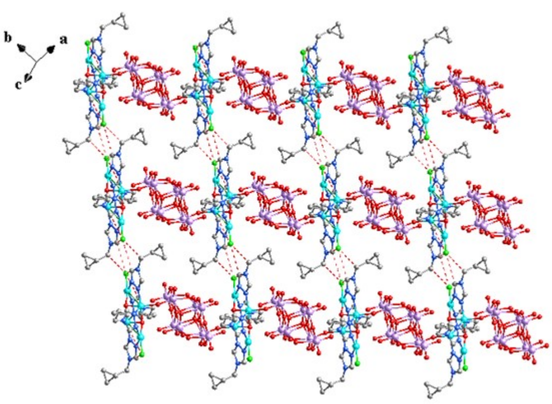

Fig. S1. The 2D supramolecular layer of complex **1**.

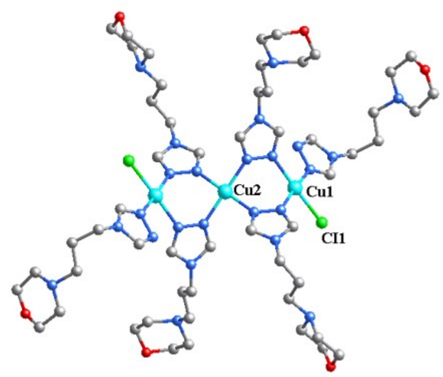

Fig. S2. The tri-nuclear Cu cluster constructed by four B-type and two A-type Tpm ligands of complex **3**.

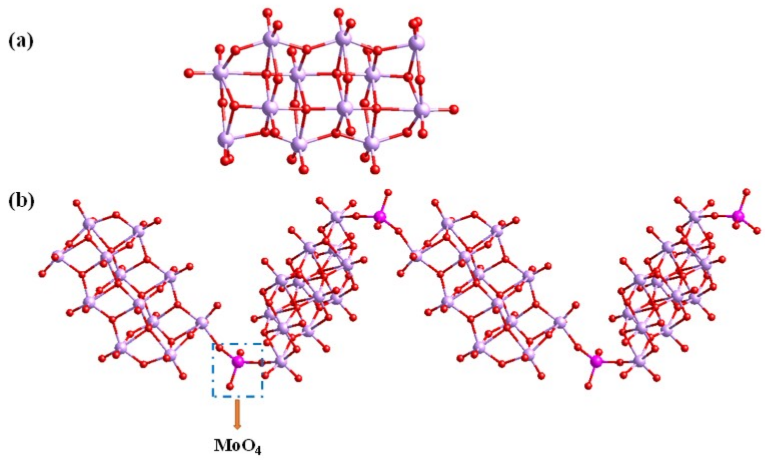

Fig. S3. (a) The $\{Mo_{12}O_{40}\}$ subunits in complex **4**. (b) The 1D inorganic chian with $\{Mo_{12}O_{40}\}$ connected by $\{MoO_4\}$ subunits through sharing the same O atoms.

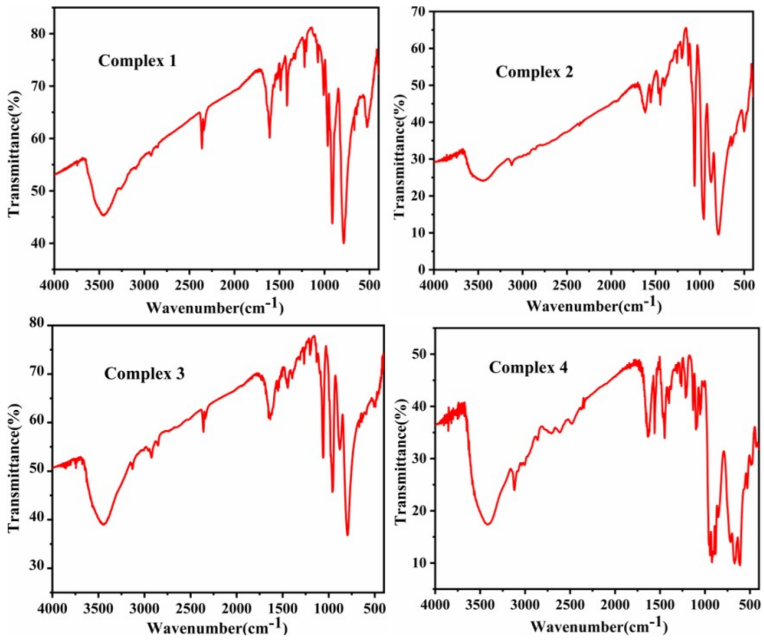

Fig. S4. The IR spectra of complexes **1−4**.

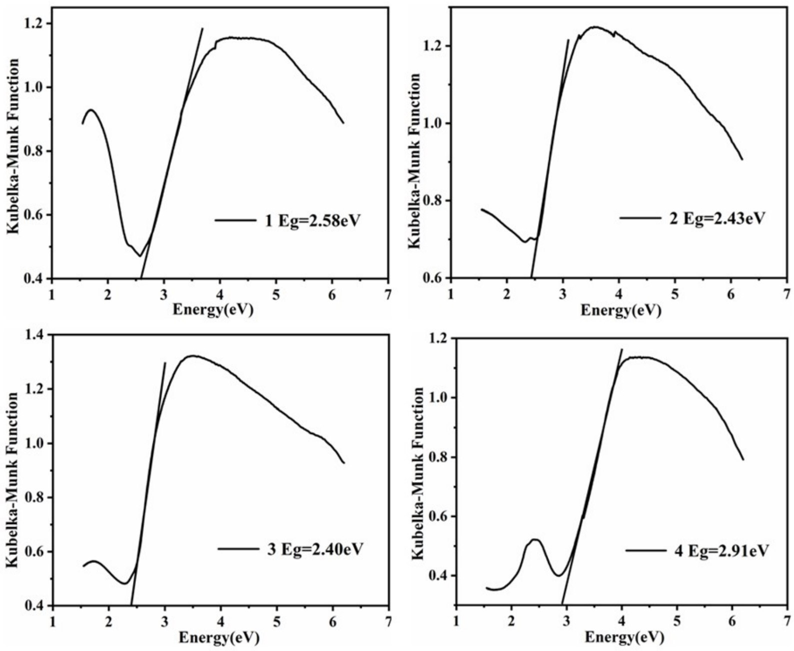

Fig. S5. Solid-state optical diffuse-reflection spectra of complexes **1−4** derived from diffuse reflectance data at room temperature.

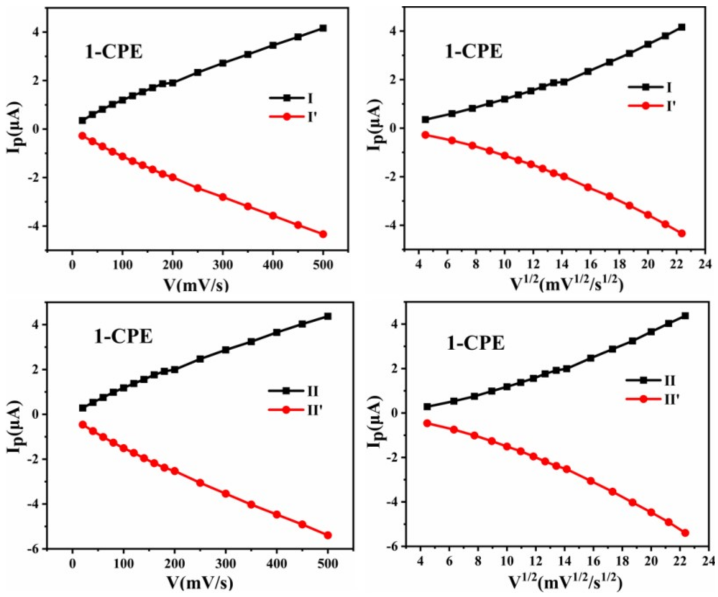

Fig. S6. The dependence of anodic peak and cathodic peak currents of **1**–CPE on ν and $\nu^{1/2}$.

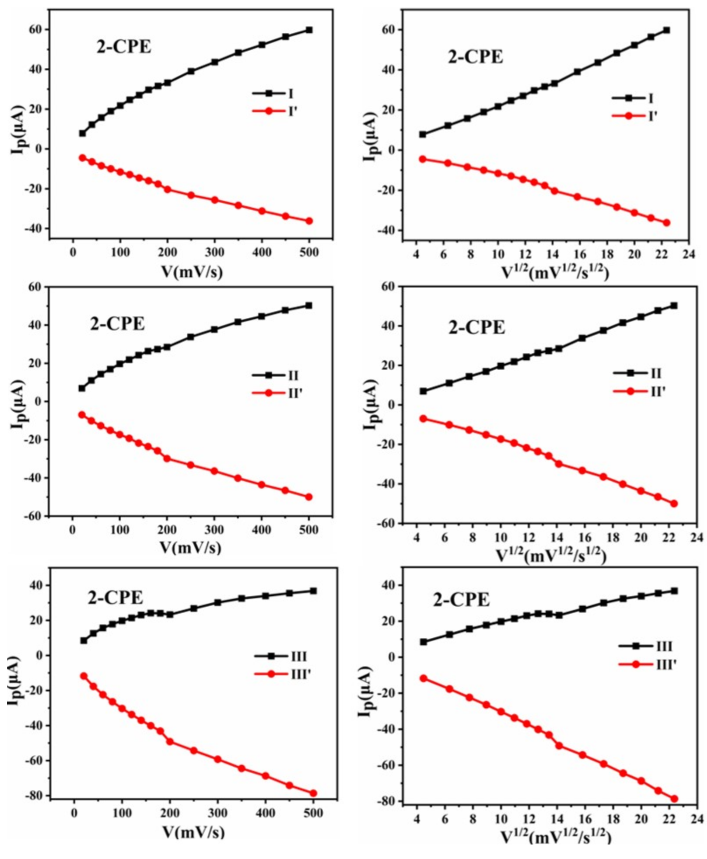

Fig. S7. The dependence of anodic peak and cathodic peak currents of **2**–CPE on ν and $\nu^{1/2}$.

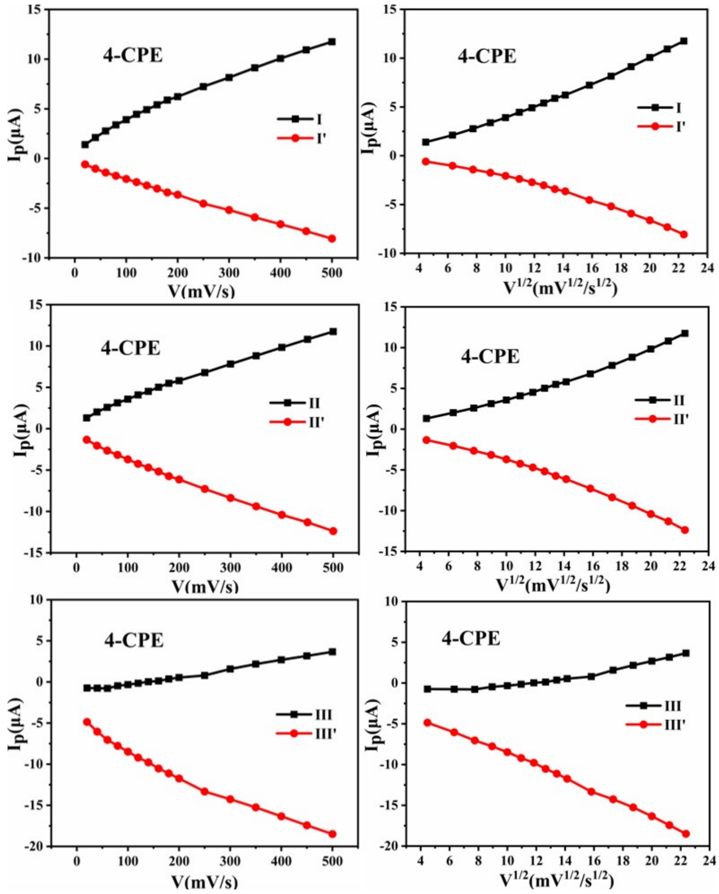

Fig. S8. The dependence of anodic peak and cathodic peak currents of **4**–CPE on ν and $\nu^{1/2}$.

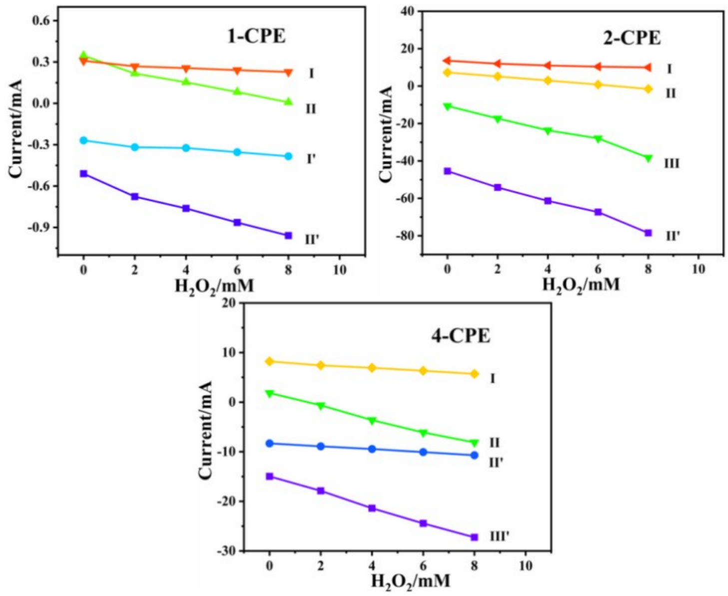

Fig. S9. Dependence of anodic and cathodic peak currents on H_2O_2 concentration for n–CPEs (n=**1**, **2** and **4**).

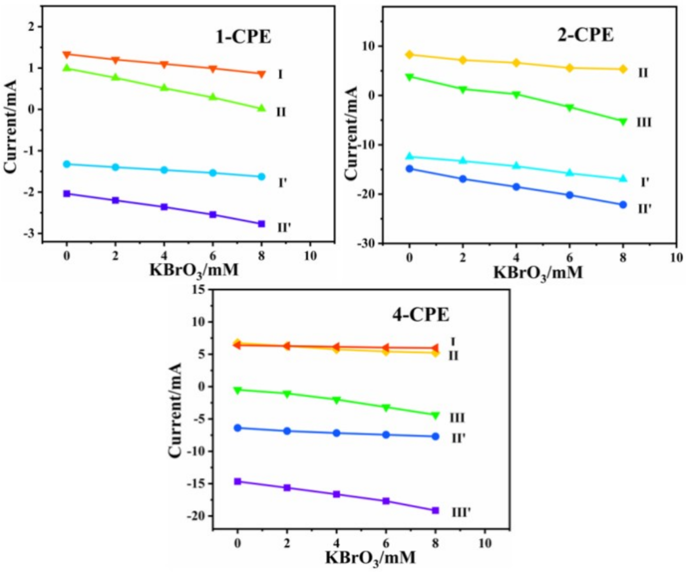

Fig. S10. Dependence of anodic and cathodic peak currents on $KBrO_3$ concentration for n–CPEs (n=**1**, **2** and **4**).

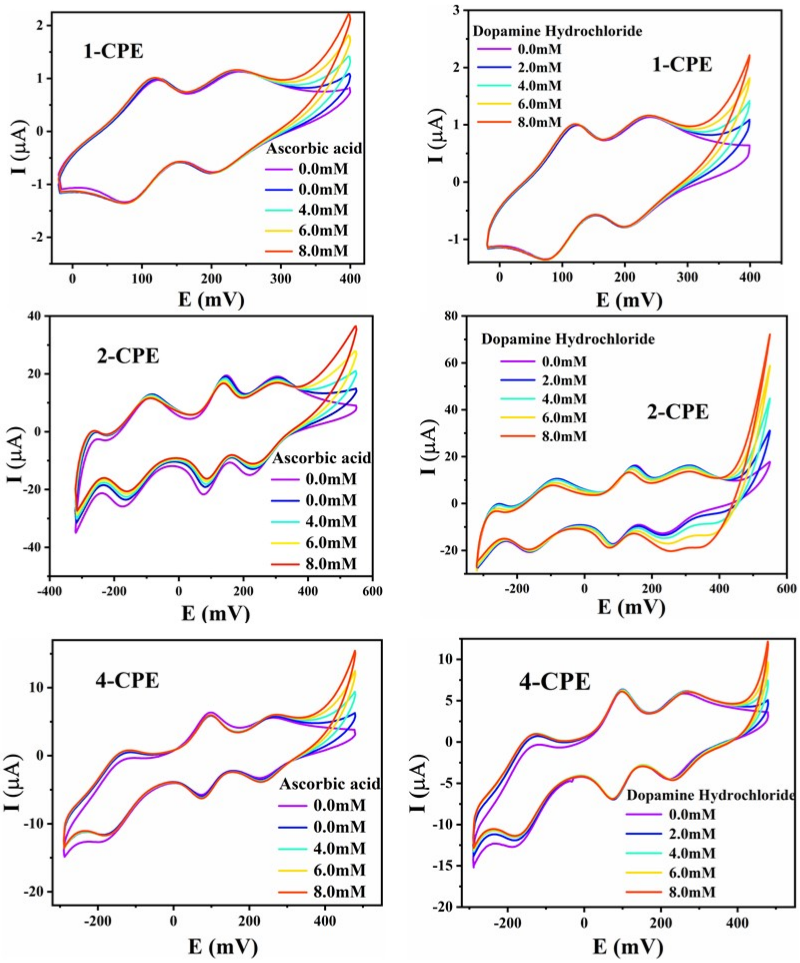

Fig. S11. Cyclic voltammograms of **1**–, **2**– and **4**–CPEs in 0.1 M H_2SO_4 + 0.5 M Na_2SO_4 aqueous solution containing 0–8 mM AA and DP. Scan rate: 200 $mV \cdot s^{-1}$.

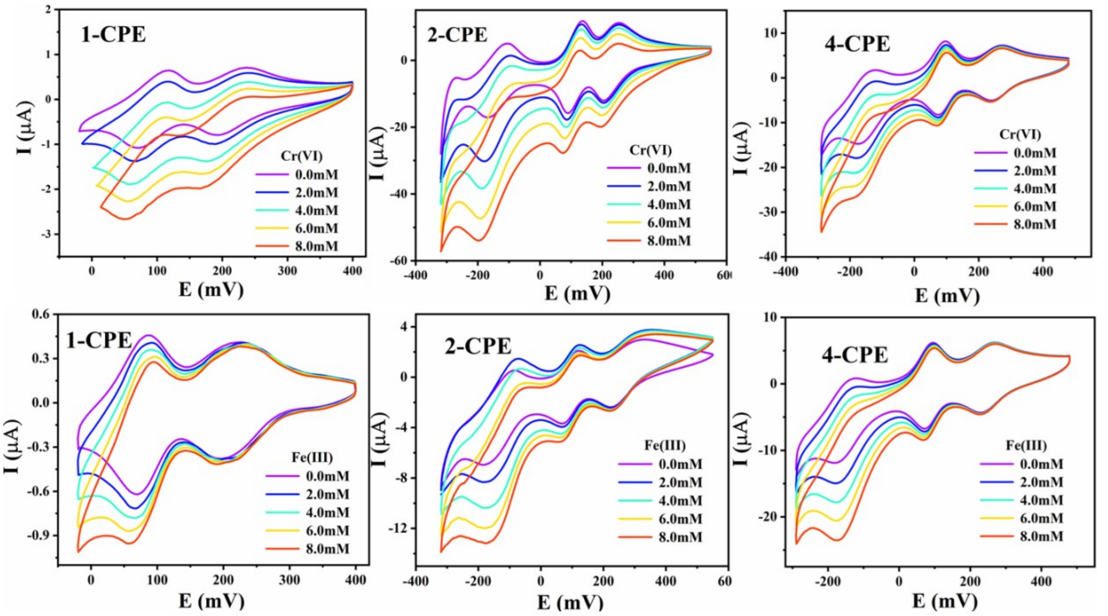

Fig. S12. Cyclic voltammograms of the **1**–, **2**– and **4**–CPEs in 0.1 M H_2SO_4 + 0.5 M Na_2SO_4 aqueous solution containing 0–8 mM Cr(VI) and Fe(III). Scan rate: 200 mV·s^{-1} .

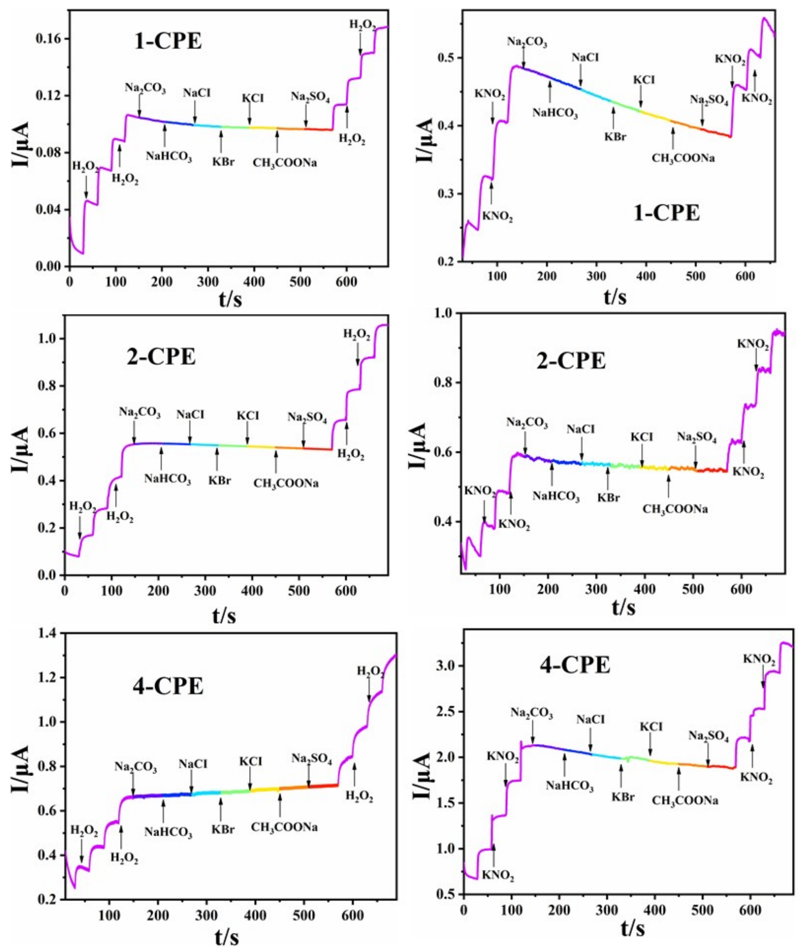

Fig. S13. Amperometric current responses of **1**–, **2**– and **4**–CPEs to NO_2^- and H_2O_2 in aqueous solution upon addition of various inorganic salts.

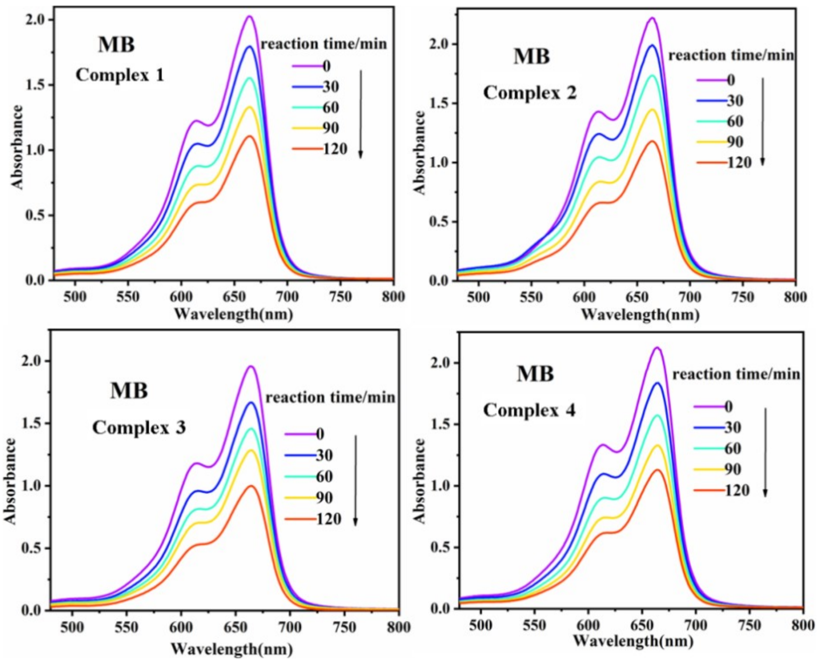

Fig. S14. The absorption spectra of MB solution during the decomposition reaction under UV irradiation with complexes **1**–**4** as catalysts.

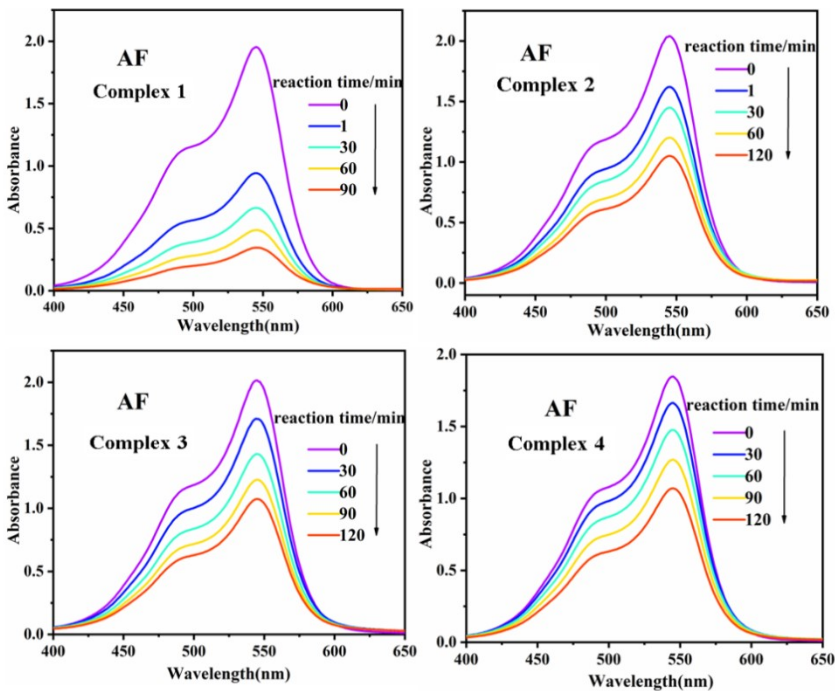

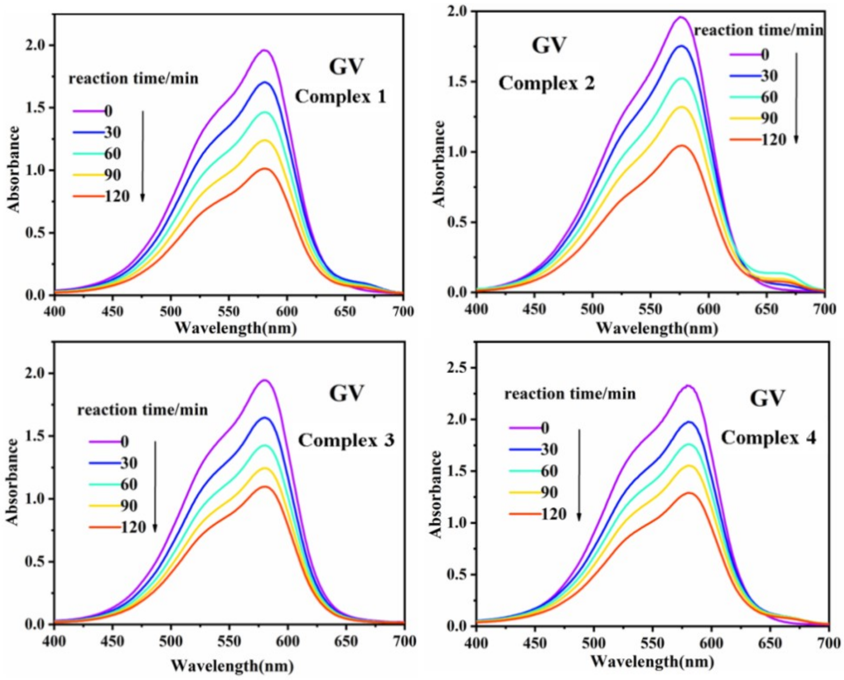

Fig. S15. The absorption spectra of GV and AF solution during the decomposition reaction under UV irradiation with complexes **1**–**4** as the catalysts.

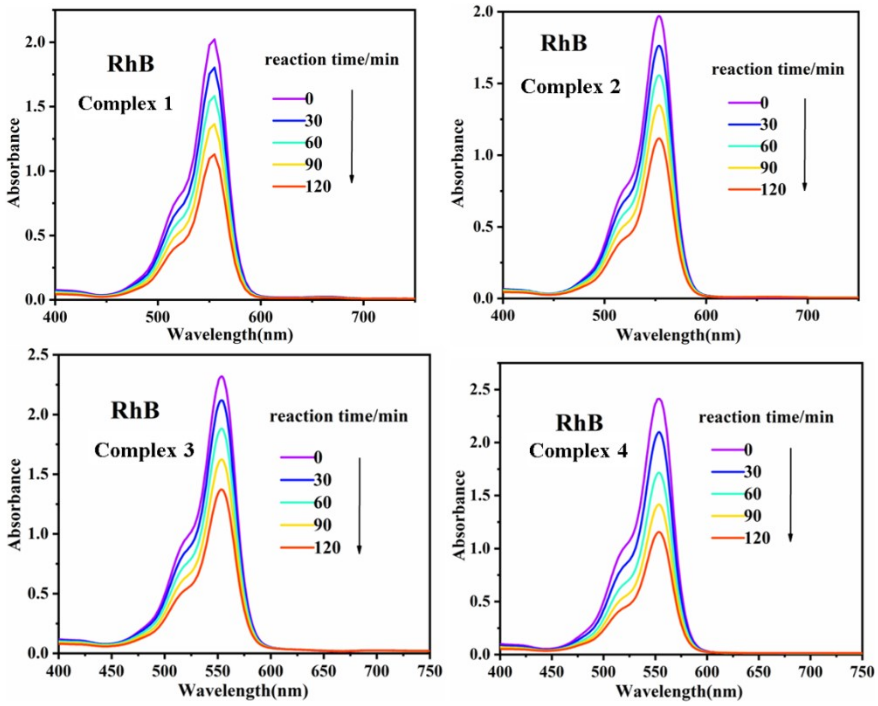

Fig. S16. Absorption spectra of the RhB solution during the decomposition reaction under UV irradiation with the complexes **1**–**4** as the catalyst.

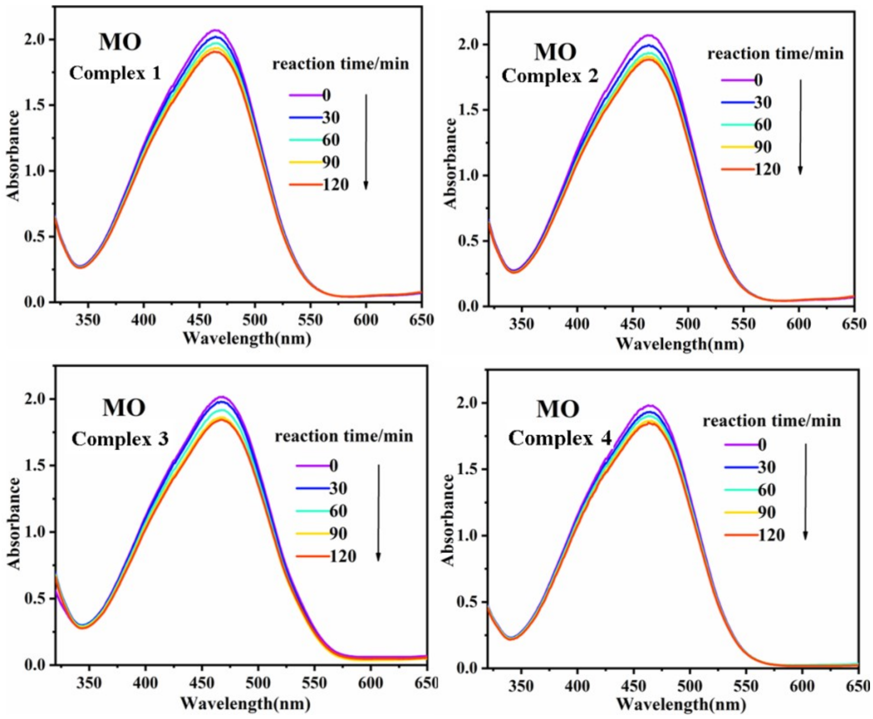

Fig. S17. Absorption spectra of the MO solution during the decomposition reaction under UV irradiation with the complexes **1**–**4** as the catalysts.

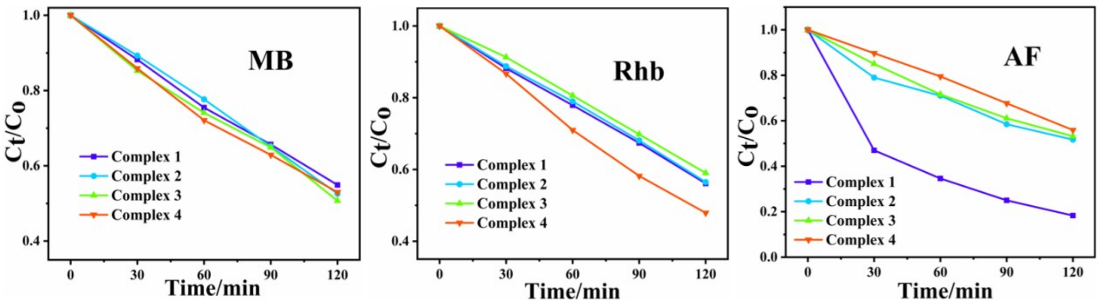

Fig. S18. The catalytic MB, RhB and AF conversion curves of complexes **1**–**4**.

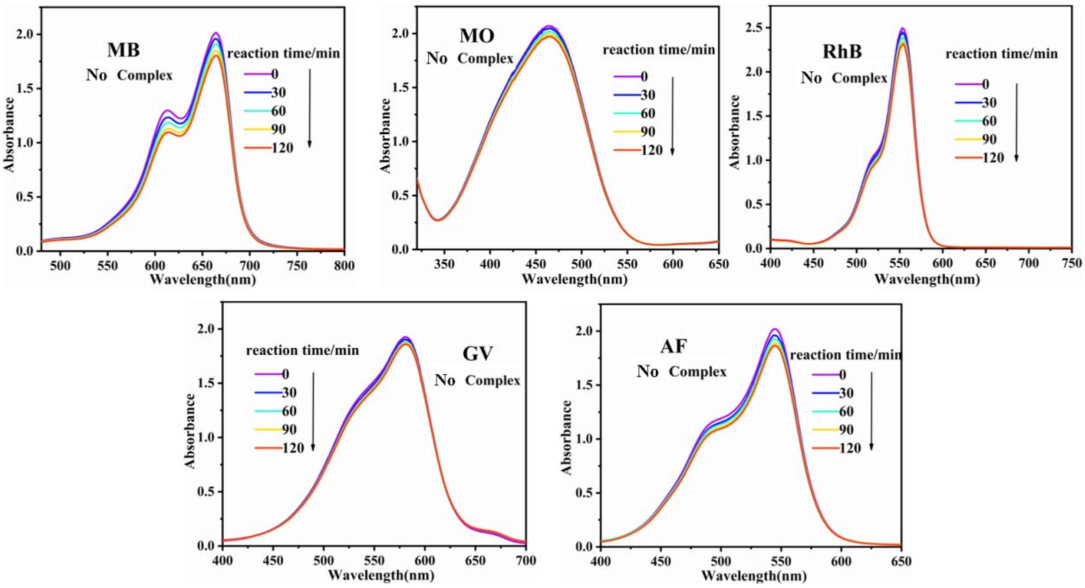

Fig. S19. Photocatalytic UV spectroscopy of organic dyes without catalysts.

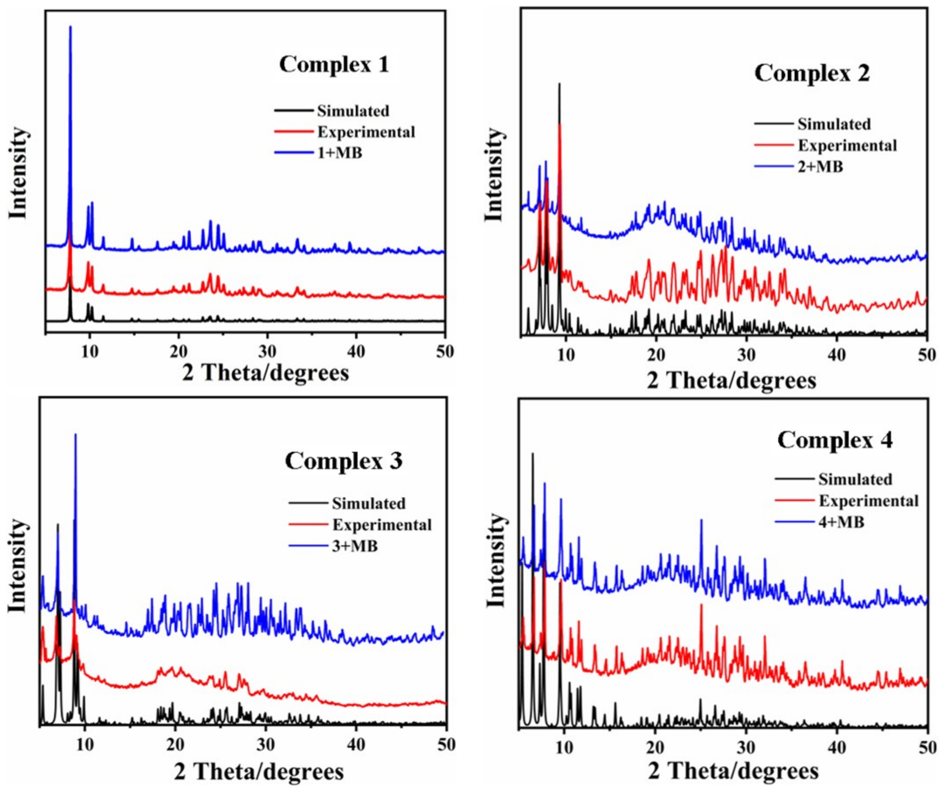

Fig. S20. The PXRD spectra of complexes **1**–**4**.

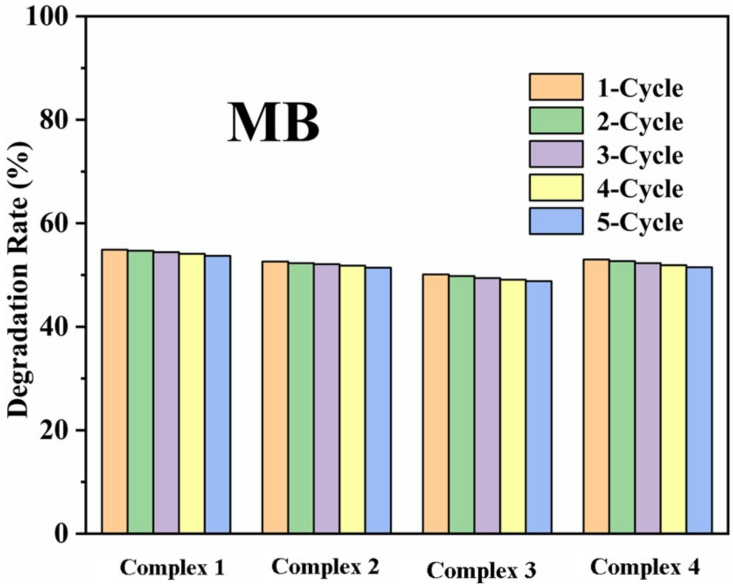

Fig. S21. Five cycles of photocatalytic degradation for MB of complexes **1–4**.

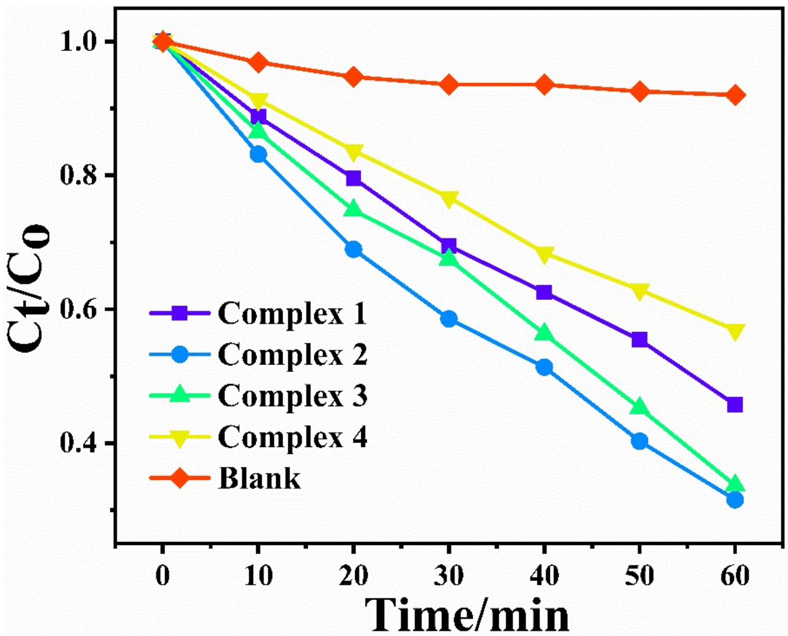

Fig. S22. Catalytic conversion curve of complexes **1**–**4**.

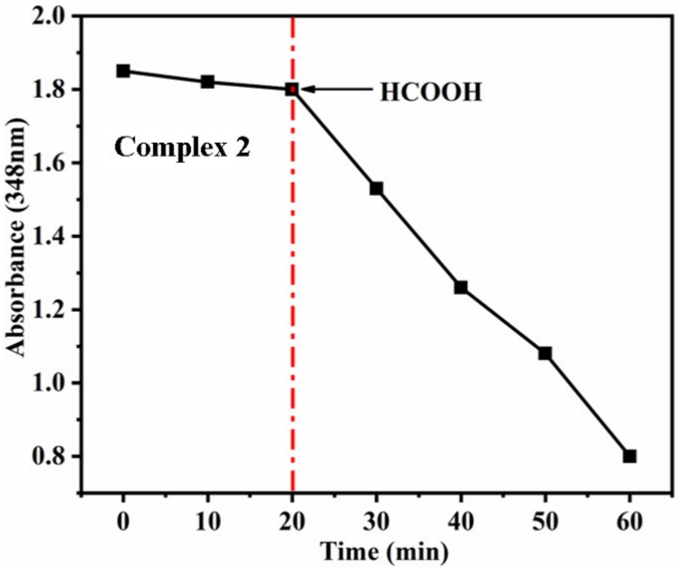

Fig. S23. Comparative experiment of complex **2** for catalytic reduction of Cr(VI): no formic acid was added in the first 20 minutes, and formic acid was added after 20 minutes.

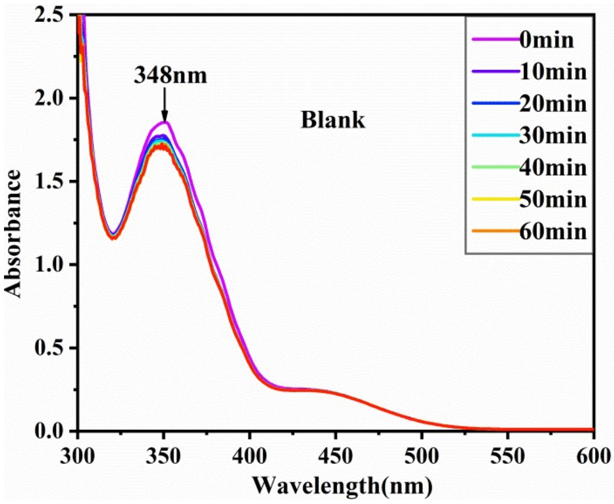

Fig. S24. UV spectra of complex **2** in Cr(VI) solution without xenon lamp irradiation.

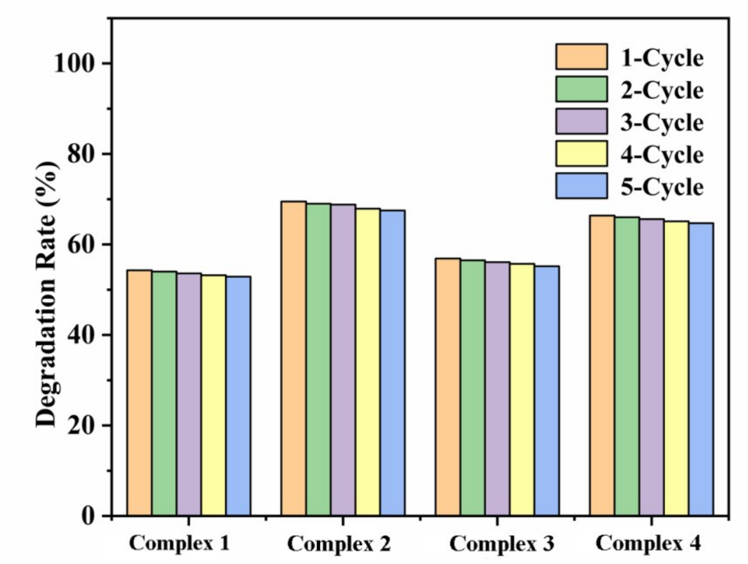

Fig. S25. Five cycles of photocatalytic reduction for Cr(VI) of complexes **1**–**4**.

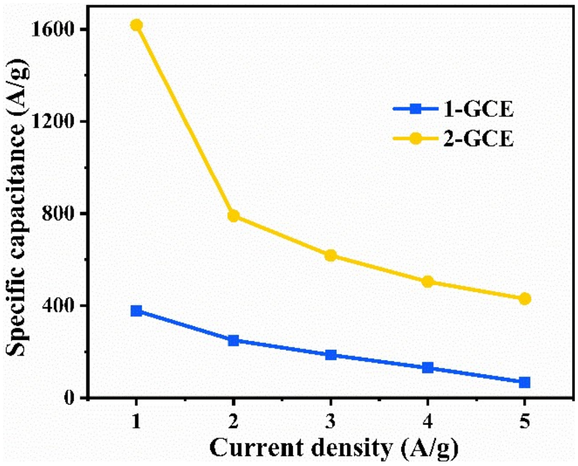

Fig. S26. The comparison of specific capacitance between **1**–GCE and **2**–GCE at different current densities.

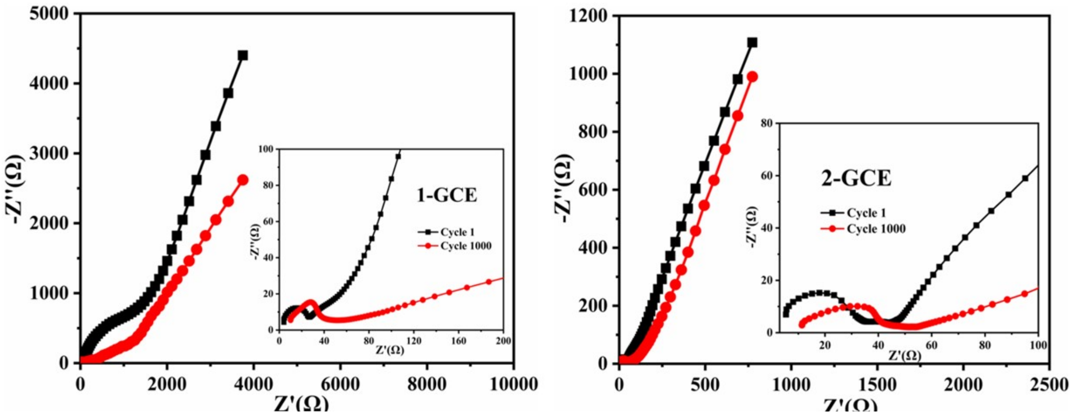

Fig. S27. Electrochemical impedance spectra of **1**– and **2**–GCE in 0.1 M H_2SO_4 solution (inset: magnified part of the high frequency range of the electrochemical impedance).

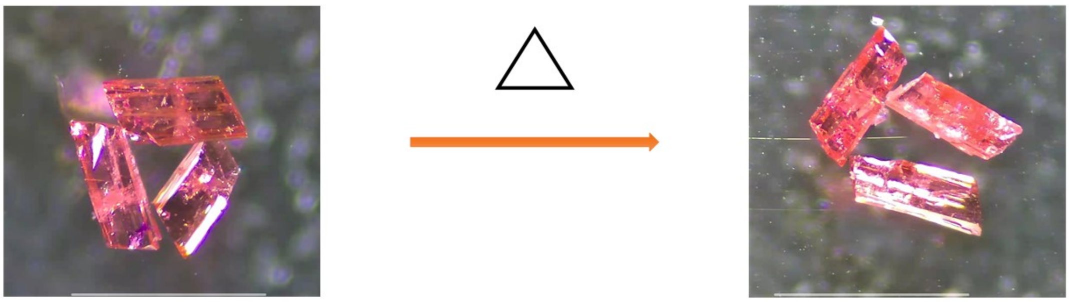

Fig. S28. Color change of complex **4** before and after thermochromism.

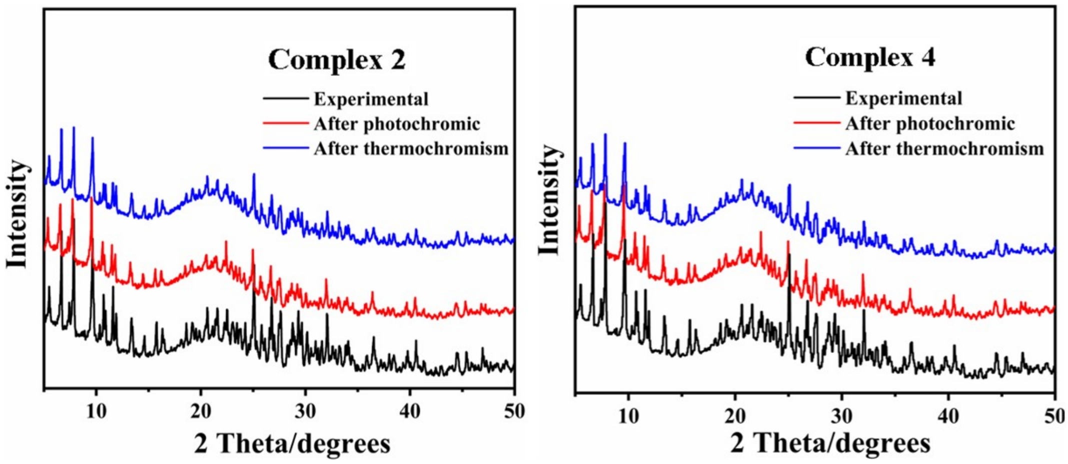

Fig. S29. PXRD before and after photochromism and thermochromism.

Table S2. Comparision of the specific capacitance values between complexes in this work and reported POMs-based electrode materials.

	Electrode material	Electrolyte	Scan rate/Current density	Specific capacitance	Ref.
1	Complex **2**	0.1 M H_2SO_4 + 0.5 M Na_2SO_4	1 A g^{-1}	1618 F g^{-1}	**This Work**
2	(PMo_{12}/PANI/TiN NWA)	1 M H_2SO_4	1 A g^{-1}	469 F g^{-1}	1
3	$[H(C_{10}H_{10}N_2)Cu_2][PMo_{12}O_{40}]$	0.5 M H_2SO_4	1 A g^{-1}	287 F g^{-1}	2
4	$[H(C_{10}H_{10}N_2)Cu_2][PW_{12}O_{40}]$	0.5 M H_2SO_4	1 A g^{-1}	153.4 F g^{-1}	2
5	$[Cu^IH_2(C_{12}H_{12}N_6)(PMo_{12}O_{40})]\cdot[(C_6H_{15}N)(H_2O)_2]$	1 M H_2SO_4	3 A g^{-1}	249 F g^{-1}	3
6	$[Cu^I_4H_2(btx)_5(PMo_{12}O_{40})_2]\cdot 2H_2O$	1 M H_2SO_4	2 A g^{-1}	237.0 F g^{-1}	4
7	$[Cu^I_4H_2(btx)_5(PW_{12}O_{40})_2]\cdot 2H_2O$	1 M H_2SO_4	2 A g^{-1}	100.0 F g^{-1}	4
8	RGO/PIL/$PMo_{12}O_{40}$	0.5 M H_2SO_4	10 mV s^{-1}	456 F g^{-1}	5
9	HT-RGO-$PMo_{12}O_{40}$	1 M H_2SO_4	10 mV s^{-1}	276 F g^{-1}	6

10	$[Cu^{II}_2(bipy)(H_2O)_4(C_6H_5PO_3)_2Mo_5O_{15}]$	0.5 M H_2SO_4	2 A g^{-1}	160.9 F g^{-1}	7

(1) L. Lu, Y. Xie, New J. Chem., 2017,**41**, 335-346. DOI:10.1039/C6NJ02368A

(2) S. Roy, V. Vemuri, S. Maiti, K. Manoj, *Inorg. Chem.*, 2018, **57**, 12078−12092. DOI:10.1021/acs.inorgchem.8b01631

(3) D. Chai, J. Xin, B. Li, H. Pang, H. Ma, K. Li, B. Xiao, X. Wang and L. Tan, *Dalton Trans.*, 2019, **48**, 13026-13033. DOI: 10.1039/C9DT02420D

(4) D. Chai, C. Gómez García, B. Li, H. Pang, H. Ma, X. Wang and L. Tan, *Chem Eng J*, 2019, **373**, 587-597. DOI:10.1016/j.cej.2019.05.084

(5) M. Yang, B. Choi, S. Jung, Y. Han, Y. Huh and S. Lee, *Adv. Funct. Mater.*, 2014, **24**, 7301-7309. DOI:10.1002/adfm.201401798

(6) J. Guevara, V. Ruiza, and P. Romero, *Phys. Chem. Chem. Phys.*, 2014, **16**, 20411-20414. DOI:10.1039/C4CP03321C

(7) B. R. Lu, S. B. Li, J. Pan, L. Zhang, J. J. Xin, Y. Chen and X. G. Tan, *Inorg. Chem.*, 2020, **59**, 1702−1714. DOI:10.1021/acs.inorgchem.9b02858